The International Supercritical CO_2 Energy Technologies Symposium
March 2 - 5, 2026, Pittsburgh, PA
Paper #035

Experimental and Numerical Investigation of Nonlinear Density Effects on Windage Loss under High-Density sCO_2

Seungkyu Lee
Ph.D. Candidate
KAIST
Daejeon, Republic of Korea

Jeong Ik Lee*
Professor
KAIST
Daejeon, Republic of Korea

	Seungkyu Lee is a Ph.D student of Nuclear and Quantum Engineering department in KAIST. He has two years of experience in designing and modeling of sCO_2 turbomachinery for various applications and operating sCO_2 Brayton cycle test loop.
	Jeong Ik Lee* is a professor of Nuclear and Quantum Engineering department in KAIST. He has been leading the development of the supercritical carbon dioxide cycle in Korea.

ABSTRACT

Accurate accounting of leakage windage in high-speed sCO_2 turbomachinery is essential because small biases in secondary-flow heating emerge through the leakage flow path and distort component matching and cycle level predictions. The windage model is calibrated with enthalpy at the final leakage station agrees with the independently determined turbine exit enthalpy. This study takes advantage of a feature of the KAIST Autonomous Brayton Cycle test loop, which is a measurable leakage path from the compressor outlet to the turbine inlet in a TAC rotor. A large dataset was assembled from various component and system experiment campaigns. Steady segments were isolated with a single-phase guard based on critical pressure or temperature and by numerical consistency checks.

A joint nonlinear least-squares fit then estimated the windage loss coefficient and density sensitivity simultaneously using an analytic Jacobian and bounded multi-start initialization. The calibrated model was able to match the conditions and retained the expected convex dependence of loss on shaft speed. The windage loss coefficient decreased relative to the baseline, while the fitted density sensitivity remained close to unity, indicating broad validity of classical scaling with modest state dependence in the densest regimes.

INTRODUCTION

Windage loss in rotating machinery is commonly modeled as linearly proportional to working-fluid density, a scaling that holds reasonably for low-density gases such as air and helium. For high-density working fluids, particularly supercritical carbon dioxide (sCO_2) near the critical point, this linear assumption can produce systematic underprediction. Reports on dense gases indicate that measured windage increasingly exceeds correlation values as density rises, implying that the conventional density exponent is often underestimated [1, 2].

The Autonomous Brayton Cycle (ABC) test loop at KAIST employs a turbine–alternator–compressor (TAC) rotor supported by active magnetic bearings. This configuration enables stable operation at high speed, pressure, and density without lubricant contamination, and is suitable for compact power systems in applications such as marine propulsion or remote installations [3]. A consequence of the magnetic bearing architecture is a finite rotor–stator gap and small leakage from the compressor outlet toward the turbine inlet. In a high-density, high-speed environment this secondary flow experiences significant frictional (windage) heating and carries the added enthalpy to the turbine [4].

During experiments on transient scenarios in the ABC test loop, discrepancies arose between simulations and observed results that were not apparent in steady-state conditions. This occurred because the power consumption of the motor driving the rotor during transient experiments differed significantly from expectations. The authors hypothesized that this was influenced by windage loss, which has the greatest impact on the power consumption of the drive motor. The state-dependent windage loss model correlation for the secondary flow, which originates downstream of the compressor and flows around the rotor, is highly influenced by density. Consequently, the research objective was established to calibrate the density multiplier.

This study explores this cumulative heating on the leakage flow path to calibrate the windage-loss model. A large, multi-campaign dataset (~133,000s of records) was integrated. Compressor outlet density spans a broad range of 200 to 450 kg/m³ where the leakage flow departures. The leakage path between compressor outlet and turbine inlet is represented by twelve stations comprising cylindrical windage and disk friction segments. The leakage flow enthalpy are initialized to the compressor outlet value and incremented station by station using loss power divided by the leakage mass flow, while pressure, temperature, and density are updated at each station. As a result, density monotonically declines downstream whereas temperature increases. For each valid case, the enthalpy at the last leakage station is finally compared with the independently measured turbine exit enthalpy to assess model fidelity.

A calibration framework is then formulated to estimate both the windage scale factor and a density exponent sensitivity under the parity between last station of leakage and turbine outlet condition. The procedure defines a residual between predicted and target enthalpies, constructs a Jacobian of that residual with respect to the unknown scale and exponent, and solves a bounded nonlinear least-squares problem [5-7]. The first Jacobian column captures sensitivity to the windage scale via a windage kernel assembled from geometry, speed, density, and leakage mass flow; the second column captures sensitivity to the density exponent through the kernel's density dependence. This approach preserves the conventional disk friction loss while allowing the cylindrical windage term to align with experimental evidence.

METHODOLOGY

2.1 Test facility the ABC test loop and test range

The ABC test loop is a simple-recuperated sCO_2 Brayton cycle equipped with a TAC rotor on magnetic bearings, a printed-circuit heat exchanger recuperator, pre-coolers (printed-circuit and shell-and-tube), cartridge heaters, high-pressure inventory tanks, and a cooling system. Barometers and thermometers are set for all major components, and flow meters are installed upstream and downstream of the compressor. Data acquisition and supervisory control run in LabVIEW, with on-line property evaluation through REFPROP. Tests cover near critical and high-density conditions at various shaft speeds up to the design point, with steady segments isolated after transient and inventory adjustments. A single-phase guard (pressure at or above the critical pressure or temperature at or above the critical temperature at the relevant location) is applied to avoid two-phase proximity. Leakage mass flow rate is calculated from the difference between the upstream and the downstream mass flow rates of the compressor as shown in Figure 1.

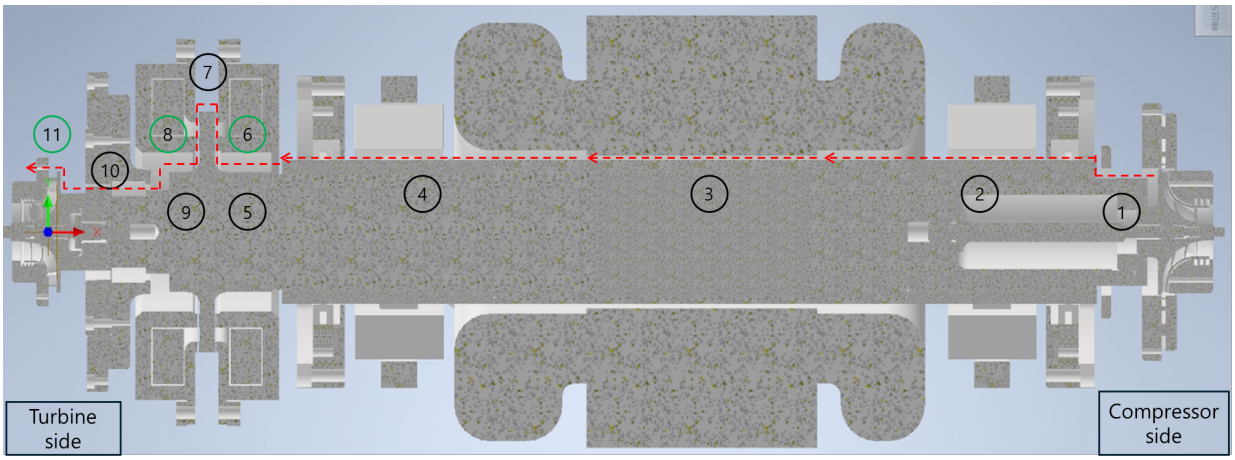

Figure 1. Leakage flow direction and windage/disk friction losses parts in the TAC

There are 12 stations and 11 segments of the leakage flow path in the TAC. The leakage flow starts from between the compressor impeller and diffuser. This leakage flows through the radial magnetic bearings, which are numbered as 2 and 4, and then the axial magnetic bearings, which are numbered as 5 to 9. 6,8 and 11 areas indicate disk friction loss parts with the green number circle, and the other parts indicates windage loss parts. Windage loss is evoked parallel to the rotational axis, and the disk friction loss is evoked perpendicular to the rotational axis as shown in Figure 2. All the dimensions of the gaps between the rotor and the stator are shown in Table 1.

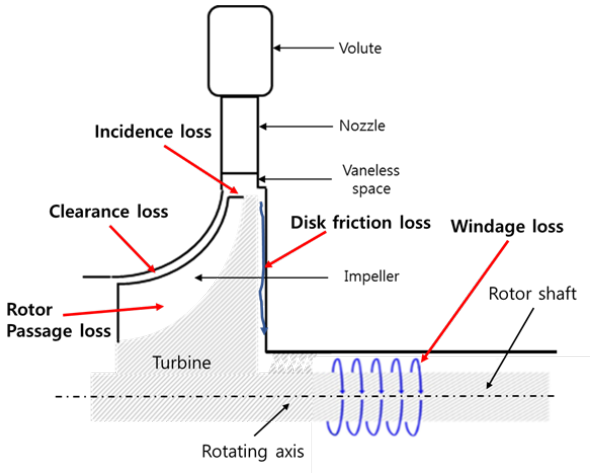

Figure 2. Losses in a turbomachinery

Table 1. Dimensions of the leakage flow area in the ABC test loop TAC

Segments	Radius (in mm)	Inner radius (in mm) (disk friction parts)	Length (in mm) (Total 456.9 mm)
1	22.35		21.1
2	30		117
3	30		94.8
4	30		127.2
5	25		28.4
6	50	25	
7	50		7
8	50	25	
9	25		16.3
10	16		45.1
11	25.8	16	

2.2 Governing equations for leakage-line accumulation

Windage power on cylindrical sections is modeled as equation 1.(Equation 1)

$$\Delta H_{windage}(i,j) = C_f \pi \rho_{ij} R_j^4 \omega_i^3 L_j$$

where i indexes operating cases and j indexes leakage stations with axial length. The corresponding specific enthalpy rise along the leakage flow is obtained by normalizing by the leakage mass flow $\dot{m}_i$ for each case.

(Equation 2) $\Delta h_{windage} = \Delta H_{windage} / \dot{m}_i$

The Daily and Nece's disk friction loss model shown in Equations 3 and 4 adopted on the segment 6, 8, 11 where viscous heating is occurring perpendicular to the rotational axis. The disk friction loss model is kept fixed while calibrating windage loss model [8].

(Equation 3) $P_{disk} = C_f \pi \rho_i (R_{j,outer}^5 - R_{j,inner}^5) \omega_i^3 / 4$

(Equation 4) $C_f = 0.0622 / Re^{0.2}$

where $\mathrm{Re} = \frac{\omega D^2}{\nu}$, wehre ω is rotational speed $\left[\frac{\mathrm{rad}}{\mathrm{s}}\right]$, D is diameter of disk [m], ν is kinematic viscousity $[\frac{\mathrm{m}^2}{\mathrm{s}}]$

The leakage flow enthalpy at final station predicted by the forward accumulation is denoted $h_{12,i}^{cur}$. A windage section that aggregates cylindrical sections is defined as Equation 5.

(Equation 5) $W_i(x) = \sum_{j \in W} \frac{\pi \rho_{ij}^x R_j^4 \omega_i^3 L_j}{\dot{m}_i}$

For arbitrary (C_f, x), the predicted j = 12 where the final station of the leakage flow enthalpy is shown in Equation 6.

(Equation 6) $\sum \Delta h_{12,i}^{windage} = \sum \Delta h_{i,disk} + C_f W_i(x)$

The turbine exit enthalpy obtained independently from measured with thermometer and barometer in ABC test loop is denoted $h_{i,turbine\ inlet}$.

The parity condition targets $h_{12,i}^{pred} \approx h_{i,turbine\ inlet}$ and define the residual

(Equation 7) $r_i(C_f, x) = \sum \Delta h_{i,disk} + C_f W_i(x) - h_{i,turbine\ inlet}$

For any fixed x, the least-squares optimal scale factor has the closed form

(Equation 8) $C_f^*(x) = \frac{W^T(x)\left(h_{turbine\ inlet} - \sum \Delta h_{i,disk}\right)}{W^T(x) W(x)}$

Equation (8) enables a fast sweep of 'x' to generate with statistical parameters Mean Absolute Error (MAE) and Root Mean Square Error (RMSE). MAE(x)/RMSE(x) curves without global optimization.

2.3 Joint estimation of scale and exponent using the Jacobian

The joint calibration solves a bounded nonlinear least-squares problem [5].

(Equation 9) $$\min\left[C_f \frac{1}{2}\sum_i r_i\,(C_f,x)^2\right], \quad subject\ to\ (C_f,x) \geq 0$$

The Jacobian of the residual vector r with respect to the parameters $\theta = [C_f, x]^\top$ is assembled analytically:

(Equation 10) $$\frac{\partial r_i}{\partial C_f} = W_i(x), \quad \frac{\partial r_i}{\partial x} = C_f \frac{\partial W_i(x)}{\partial x}$$

(Equation 11) $$\frac{\partial W_i(x)}{\partial x} = \sum_{j\in W} \frac{\pi \rho_{ij}^{x} \ln \rho_{ij} R_j^4 \omega_i^3 L_j}{\dot{m}_i}$$

Gauss–Newton or trust-region updates with the analytic Jacobian are employed. At the solution $\hat{\theta} = [\hat{C}_f, \hat{x}]$, the parameter covariance is approximated by the normal-equation linearization which provides standard errors and parameter correlation [6, 7].

(Equation 12) $\widehat{Cov}(\hat{\theta}) \approx \hat{\sigma}^2 (J^T J)^{-1}$, where $\hat{\sigma}^2 = \frac{\|r(\theta)\|_2^2}{N-2}$

RESULTS

Figure 3 shows the time series of the enthalpy difference between the final leakage station and the turbine exit using conventional disk friction loss and windage loss models as shown in Equations 3,4, and 13. Several bands exhibit a clear offset, and some negative spikes appear during inventory adjustments and unfiltered systemic dynamic transient situations. Most of the dataset cases, the predicted enthalpy are higher than measured turbine inlet enthalpy. It means that the original windage loss model is overestimating the windage loss phenomena. These baseline features motivate a calibration strategy that enforces parity between the last leakage station and the independently evaluated turbine-exit enthalpy.

(Equation 13) $P_{wind,original} = 0.001\pi\rho_{ij} R_j^4 \omega_i^3 L_j$; Original windage loss model

Figure 4 shows the direct parity scatter of predicted last-station enthalpy versus turbine-exit enthalpy. The points form a tilted cloud around the 1:1 line, with most cases lying inside the ±10% corridors but a noticeable subset drifting outside, especially at higher enthalpy. To understand the origin of these deviations, Figure 5 shows the sum of disk friction and windage loss against shaft speed. The overall trend is convex, but distinct branches appear in operating bands where the leakage density is high highlighted by black circles. Coloring the loss sum–speed map by compressor-outlet density explains the apparent “spikes” into consistent state clusters. Flagged points concentrate at higher density and lower temperature, which is consistent with stronger viscous loss in dense sCO_2. Figure 6 also confirms this interpretation. In Figure 6, x-axis indicates leakage inlet density and y-axis indicates probability density function (PDF). This histogram shows that outliers occur at substantially higher outlet densities than inliers, and the histogram exhibits multiple peaks that reflect the campaign-level operating envelopes. Collectively, these diagnostics show that a strictly linear density scaling is

inadequate over the full range and that the effective density sensitivity increases in high-density regimes.

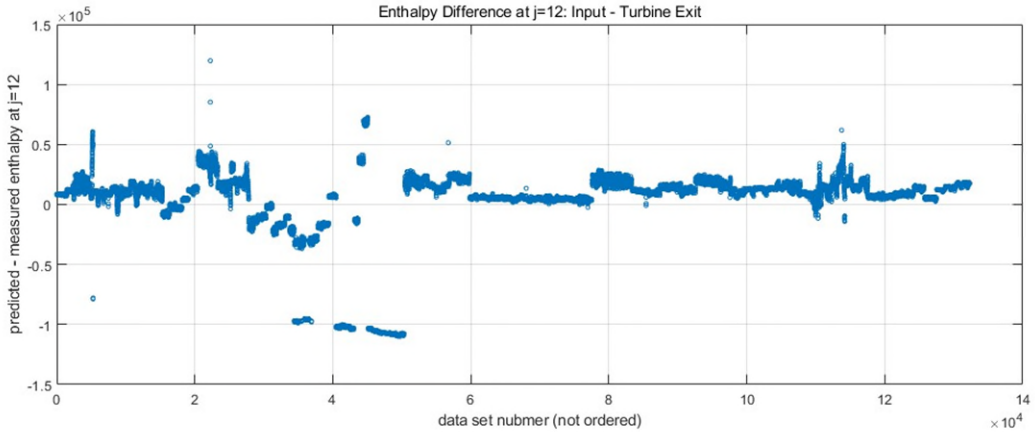

Figure 3. Time series view of enthalpy difference between estimated and measured

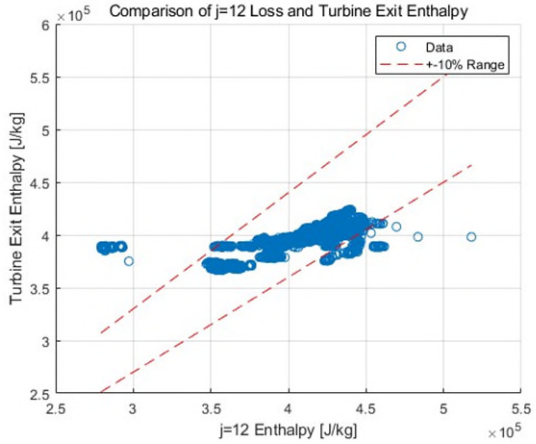

Figure 4. Scattering view of enthalpy difference between estimation and experiment

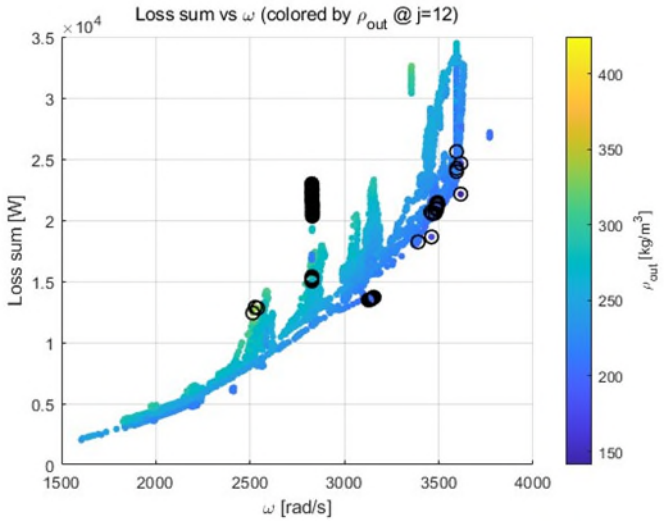

Figure 5. rotor speed and Loss sum colored by leakage density (outlier density cases are highlighted by dark circles)

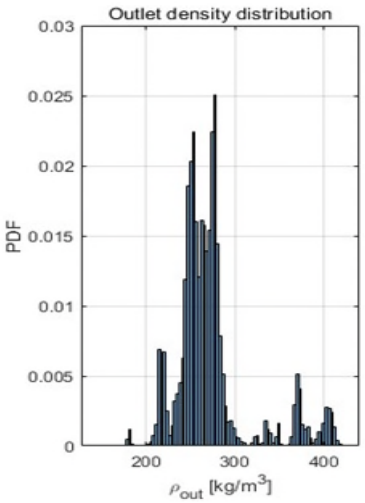

Figure 6. Leakage inlet (compressor outlet) density histogram

Applying the Jacobian based calibration that minimizes the parity residual brings the predictions into much closer agreement with measurements. In Figure 7, the parity scatter contracts toward the 1:1 line, the cloud becomes more symmetric. Figure 8 proves the improvement in the time domain: the error series centers near zero and its spread decreases across most rpm bands, with the largest reductions in bands that were previously biased negative. Figure 9 presents an alternative parity view that emphasizes the calibrated density exponent. Figure 10 shows smaller dispersion and fewer extreme excursions of no more than 2kJ/kg for most cases. These outcomes indicate that jointly tuning the windage scale and the density exponent removes most of the systematic bias. The corresponding calibrated parameters are summarized in Table 2 and Equations 14 and 15.

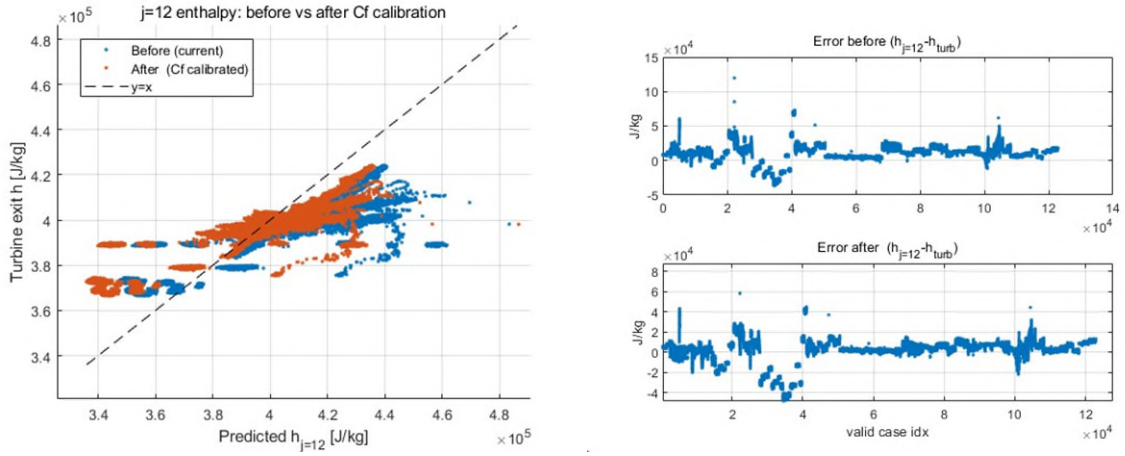

Figure 7, 8. Before and after Cf calibration scattering plot and residual plot of time series

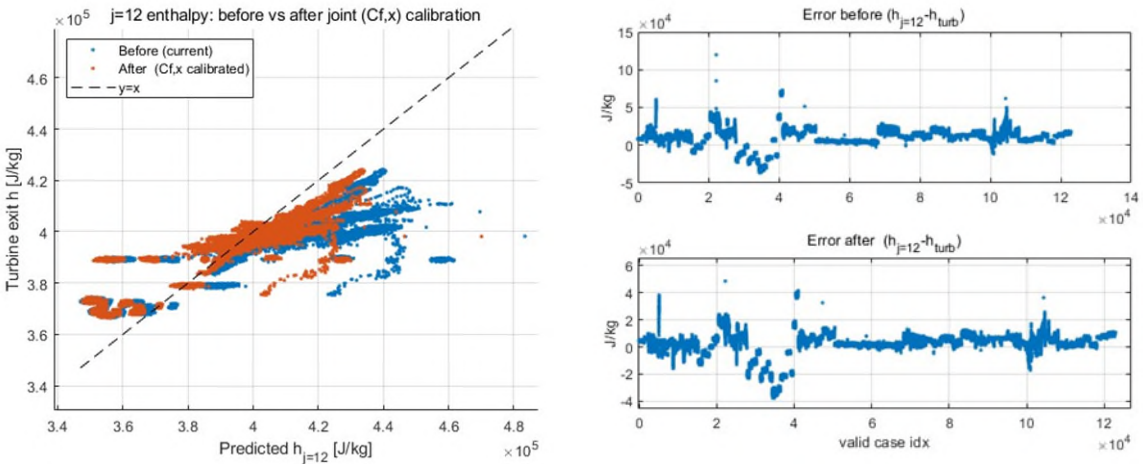

Figure 9, 10. Before and after Cf and density exponent x calibration scattering plot and residual plot of time series

Table 1. Loss model coefficients and density exponent of original and calibrated models

Coefficient	Original model	Cf calibration	Cf and x Calibration
Cf	**$10*10^{-4}$**	**$6.23*10^{-4}$**	**$1.98*10^{-6}$**
x (density exponent)	**1**	**1**	**1.92**
Mean Absolute Error (in J/kg)	**13,522**	**8,544**	**6,430**
Root Mean Square Error (in J/kg)	**15,994**	**12,528**	**9,197**

(Equation 14) $$P_{wind,calib\,1} = 6.23 * 10^{-4} \pi \rho_{ij} R_j^4 \omega_i^3 L_j$$

(Equation 15) $$P_{wind,calib\,2} = 1.98 * 10^{-6} \pi \rho_{ij}^{1.92} R_j^4 \omega_i^3 L_j$$

DISCUSSION

Figure 4 (parity scatter) indicates a systematic bias in the baseline: most points lie within the ±10% corridors, substantial cases escape from the 1:1 line at higher enthalpy, implying under-estimated density sensitivity. Figure 5 attributes much of this bias to operating bands with high leakage density. The loss–speed trend is globally fitted but splits into branches as the state moves deeper into the dense regime. Coloring by compressor-outlet density collapses the apparent spikes into coherent state clusters, and Figure 6 confirms that outlier-flagged cases occupy substantially higher density conditions than other measured data. These diagnostics show that linear density scaling for windage loss modeling is not adequate across the full envelope and that the effective density sensitivity strengthens with density.

A Jacobian-based calibration that minimizes the parity residual corrects most of the bias

while preserving the disk friction loss model. After calibration, Figure 7 shows the parity cloud contracting toward the 1:1 line with far fewer points not collapsed. Figure 8 shows the error series re-centering near zero with reduced spread. A second parity view that emphasizes the density-exponent fit (Figure 9) and its companion error trace (Figure 10) confirm smaller dispersion and fewer extreme excursions. Quantitatively, the step that adjusts only the windage scale reduces MAE from 13,522 to 8,544 J/kg (≈37%) and RMSE from 15,994 to 12,528 J/kg (≈22%). The full joint fit (windage scale + density exponent) reduces MAE to 6,430 J/kg (≈53%) and RMSE to 9,197 J/kg (≈43%), demonstrating that both parameters are needed for dense-regime parity. Table 2 summarizes the parameter evolution.

The calibrated pair reported in Table 2 shows a strong trade-off between the windage scale and the density exponent: when the exponent rises from 1 to 1.92, the fitted scale decreases by orders of magnitude while delivering comparable parity. Residual structure that remains at the highest densities implies weak state dependence that a single global exponent cannot fully capture. Two light-weight extensions are natural next steps: a weak state-aware exponent (e.g., exponent as a low-order function of outlet density or temperature) and a composite sensitivity that admits viscosity together with density. Both preserve the current kernel and disk-friction model while targeting the densest bands highlighted in Figures 5 and 6.

SUMMARY

This study calibrates the windage loss model with experiment dataset of a high-speed sCO_2 TAC. The last leakage station enthalpy must match the independently evaluated turbine-exit enthalpy. A large multi-campaign dataset is filtered with a single-phase guard and steady state quality checks, then processed through an eleven segments leakage model that accumulates specific enthalpy rise while updating state variables station by station. Baseline parity reveals systematic offsets and dense regime branches in the loss speed map, showing that a linear density scaling is insufficient. A two-layer estimation closed-form scale at fixed exponent followed by a bounded Jacobian-based joint fit reduces MAE by about 53% and RMSE by about 43% relative to the baseline, while preserving the convex loss–speed trend and the disk-friction correlation. The post calibration parity cloud tightens around the 1:1 line and error series re-center near zero across rpm bands. The fitted parameters exhibit a scale exponent trade-off typical of power-law identification reporting parameter uncertainties and correlation will make this transparent. Residuals that persist at the highest density cases suggest modest extensions. The resulting workflow is lightweight, reproducible, and directly reusable for future campaigns. It provides a single scalar target per case, integrates with the existing post-processing, and maintains physics fidelity while extending accuracy into dense, near-critical operating regimes.

REFERENCES

[1] Span, R., Wagner, W., “A New Equation of State for Carbon Dioxide Covering the Fluid Region,” *J. Phys. Chem. Ref. Data* (1996).

[2] Owen, J. M., Rogers, R. H., *Flow and Heat Transfer in Rotating-Disc Systems*.

[3] Kim, D. K., 2019, Study of Magnetic Bearing Instability for KAIST Micro Modular Reactor Application, KAIST, Daejeon, South Korea.

[4] Vrancik, J. E., 1968, Prediction of Windage Power Loss in Alternators, NASA, Washington, DC, Report No. TN D-4849.

[5] Cleveland, W. S., “Robust Locally Weighted Regression and Smoothing Scatterplots (LOWESS),” *JASA* (1979).

[6] Moré, J. J., “The Levenberg–Marquardt Algorithm: Implementation and Theory,” *Lecture Notes in Mathematics* (1978).

[7] Rousseeuw, P. J., Leroy, A. M., *Robust Regression and Outlier Detection*.

[8] Daily, J. W., Nece, R. E., “Chamber Dimension Effects on Induced Flow and Frictional Resistance of Enclosed Rotating Disks,” *ASME J. Basic Eng.* (1960).